Electronic Supplementary Information (ESI)

A dinuclear Cd^{II} cluster-based stable luminescent metal-organic framework for the consecutive and visual detection of $H_2PO_4^-$ and OCN^-

Na Lu, Li Wang, Teng-Fei Zheng,* Yan Peng, Sui-Jun Liu* and He-Rui Wen

School of Chemistry and Chemical Engineering, Jiangxi Provincial Key Laboratory of Functional Molecular Materials Chemistry, Jiangxi University of Science and Technology, Ganzhou 341000, Jiangxi Province, P.R. China

*Corresponding authors. E-mail: sjliu@jxust.edu.cn (S.-J. Liu), zhengtengfei0628@163.com (T.-F. Zheng).

Materials and instrumentations

All chemical reagents were obtained from commercial sources and used without further purification. Notably, H_2BTDB was purchased by Jilin Chinese Academy of Sciences -Yanshen Technology Co., Ltd. Thermogravimetric analysis (TGA) was performed under a N_2 flow at a heating rate of 10 °C min^{-1} from 25 to 1000 °C on a NETZSCH STA2500 thermal analyzer. The powder X-ray diffraction (PXRD) patterns were recorded by Rigaku MiniFlex 600. The simulated PXRD pattern of single-crystal data was obtained using the Mercury (Hg) software, which is freely available on the Internet at http://www.iucr.org. IR spectra in the range of 4000-400 cm^{-1} were collected with KBr particles on a Bruker Alpha FT-IR spectrometer. X-ray photoelectron spectrum (XPS) was obtained with an Axis Ultra DLD spectrometer. The fluorescence measurements were carried out on an F4600 (Hitachi) fluorescence spectrophotometer. The UV-vis absorption spectra for all samples were collected on a UV-2550 (SHIMADZU) spectrophotometer.

Crystal Description

X-ray single-crystal diffraction data of **JXUST-47** were recorded on a Bruker D8 QUEST with ω-scan pattern and Mo-Kα radiation (λ = 0.71073 Å). The structure is solved by using direct methods with SHELXTL software and refined using full-matrix least-squares.[S1] The anisotropic thermal parameters on non-hydrogen atoms are refined by F^2. This structure is based on weak and highly inconsistent data. Fig. S1 shows that there exist electrons or unresolved atoms in **JXUST-47**. As shown in Fig. S2, **JXUST-47** there exist numerous outliers. The *R* merge rises above 15% at about 1.4 (Fig. S3). As shown in Fig. S4, the I/σ drops below 3 at $2\theta = 41$. The ORTEP drawing of **JXUST-47** is shown in Fig. S5. During the collection of crystal data, scan width is 0.50 and exposure time is 10 s. The exposure time of 10 s may not be optimal, and the reason for the weak data is merely the limited crystal quality and the short exposure time.

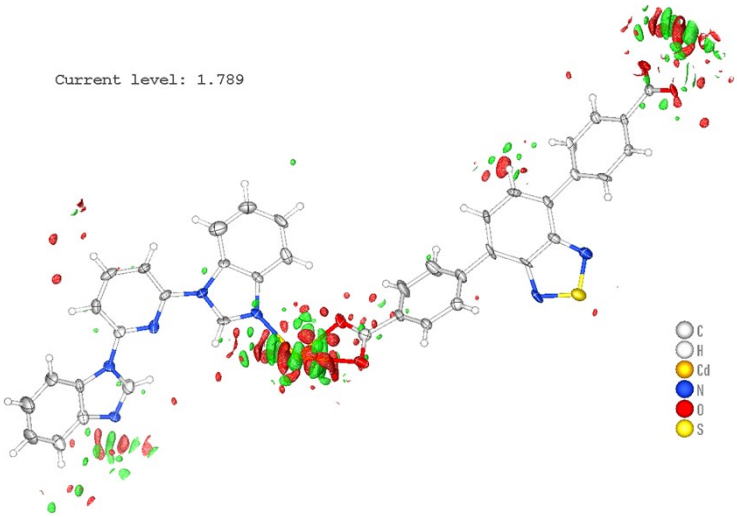

Fig. S1 The residual density map of **JXUST-47**.

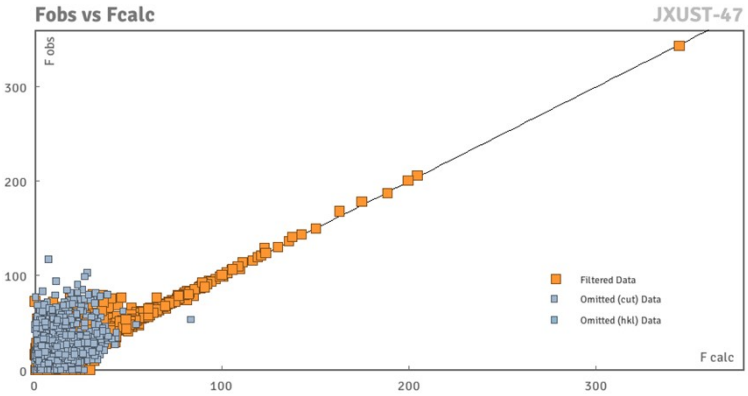

Fig. S2 The F obs vs F calc plot of **JXUST-47**.

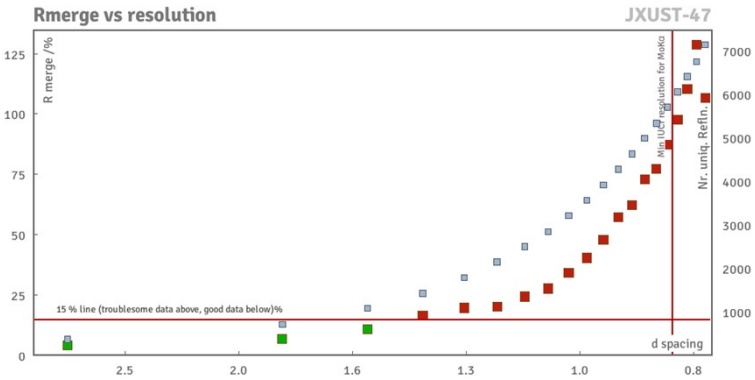

Fig. S3 The plot of *R* merge vs resolution of **JXUST-47**.

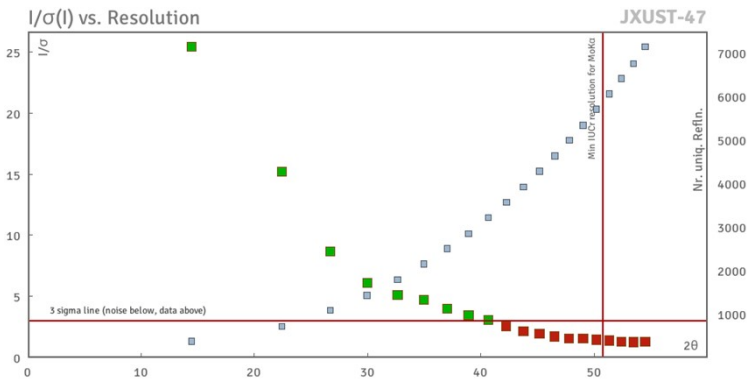

Fig. S4 The plot of I/σ(I) vs resolution of **JXUST-47**.

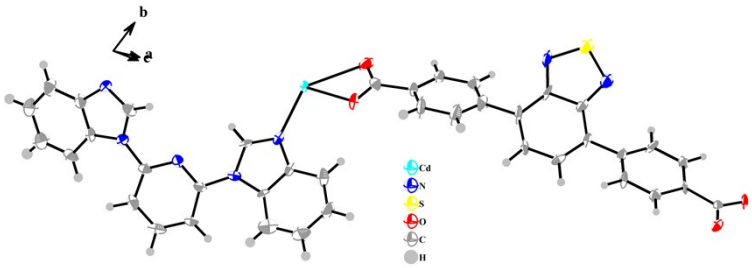

Fig. S5 The ORTEP drawing of **JXUST-47**.

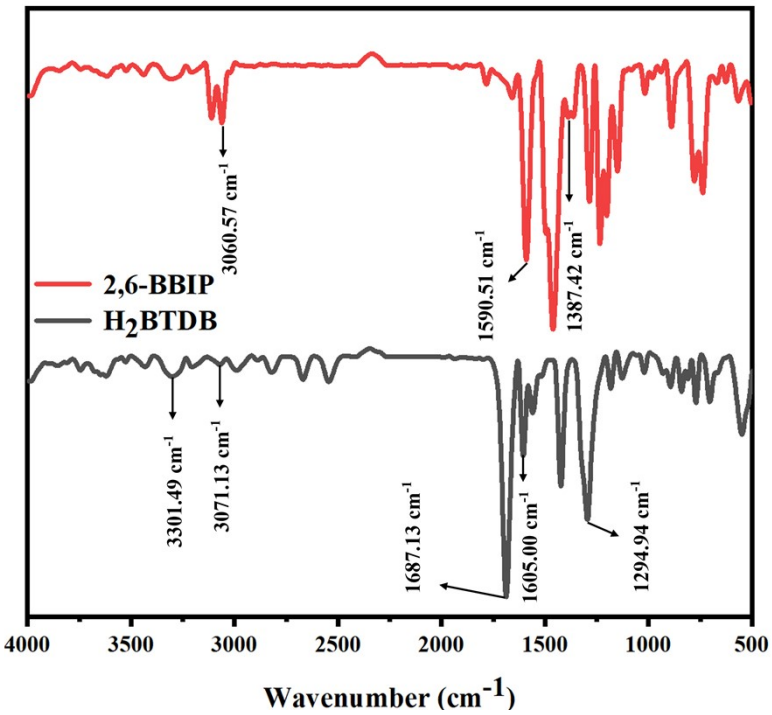

Fig. S6 The IR spectra of 2,6-BBIP and H_2BTDB.

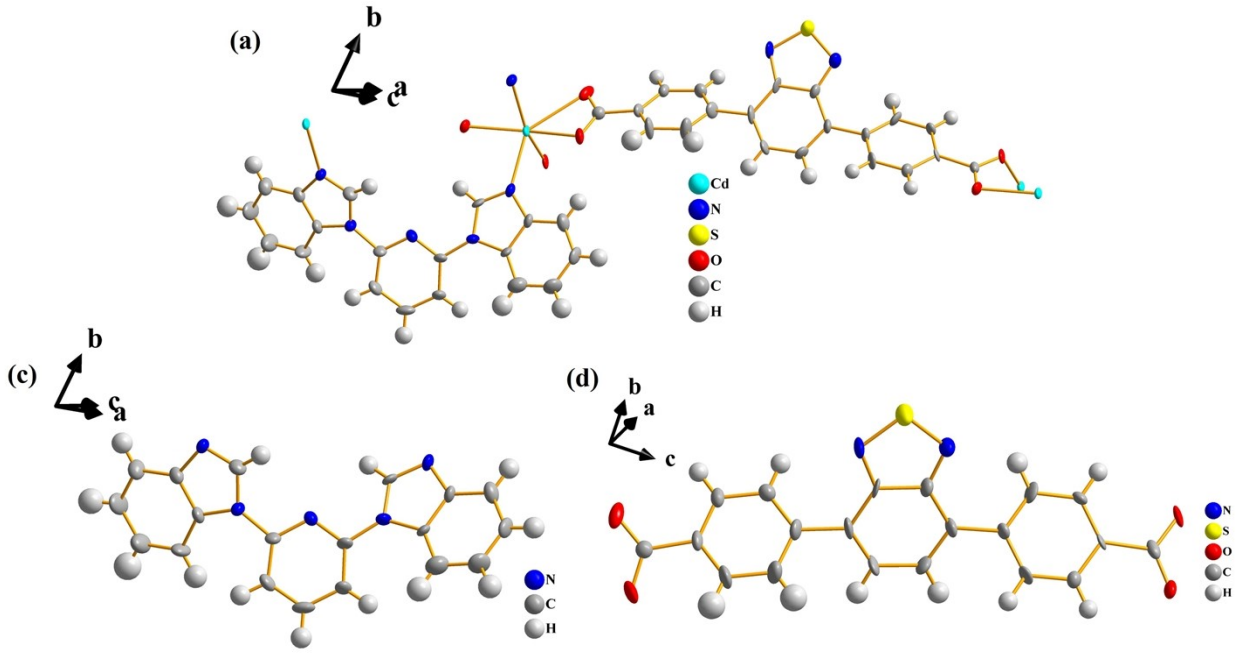

Fig. S7 The ellipsoid diagrams of (a) **JXUST-47**, (b) 2,6-BBIP and (c) H_2BTDB.

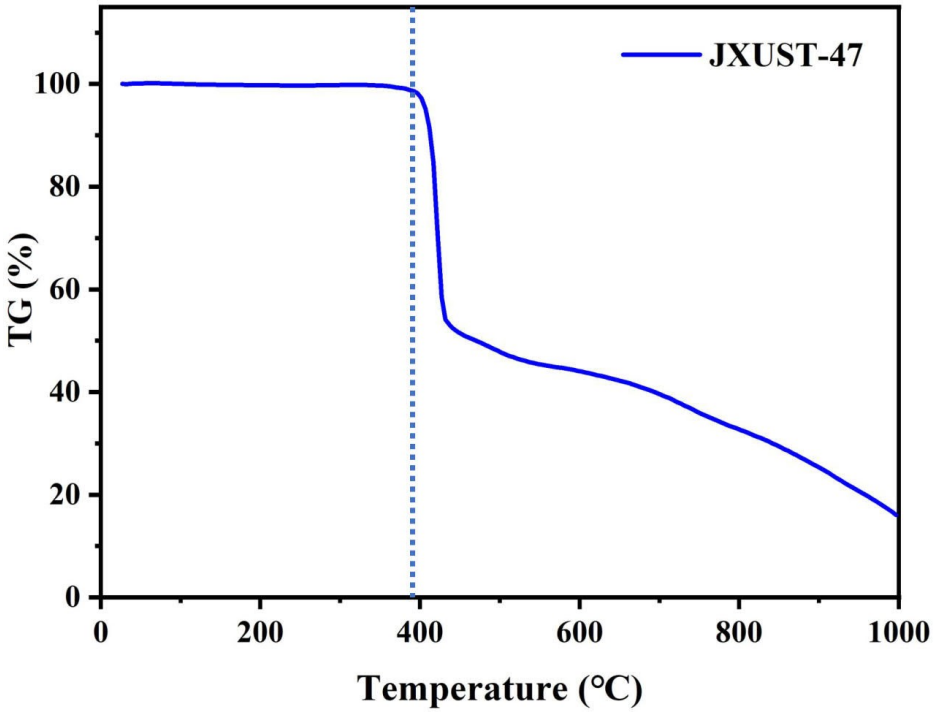

Fig. S8 The TGA curve of **JXUST-47**.

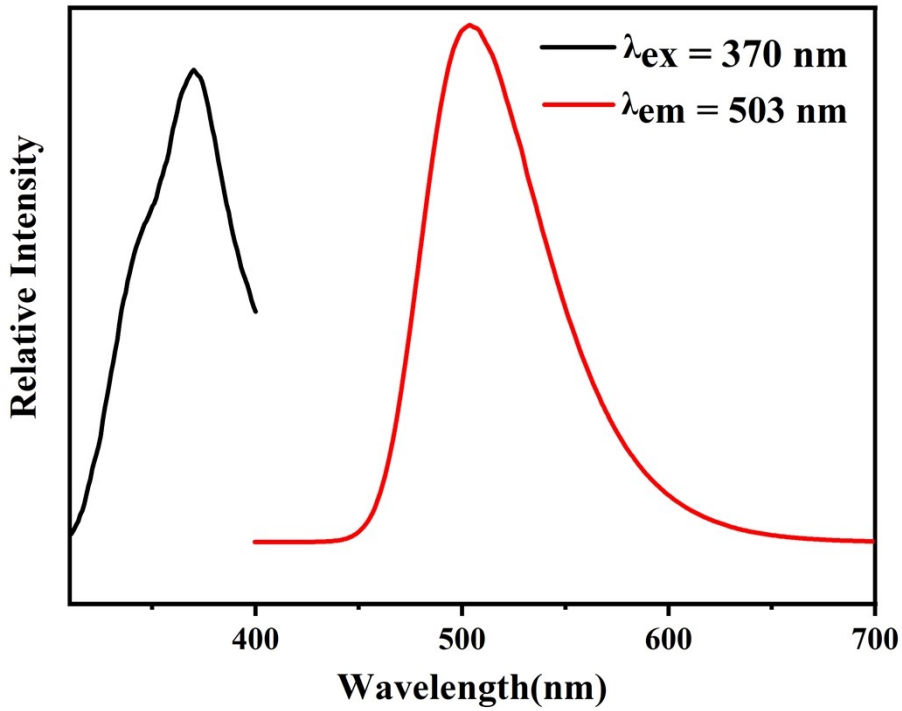

Fig. S9 The solid-state excitation and emission spectra of **JXUST-47**.

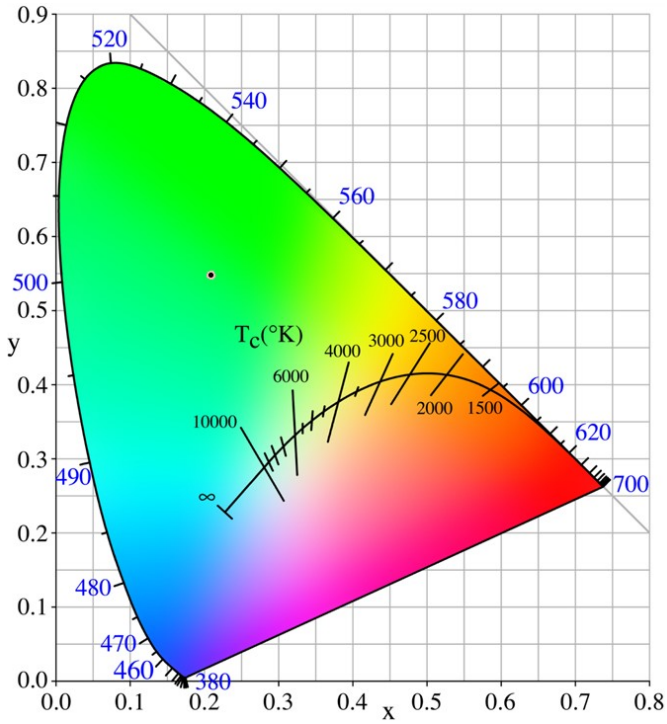

Fig. S10 CIE chromaticity diagram displaying the color coordinate of **JXUST-47**.

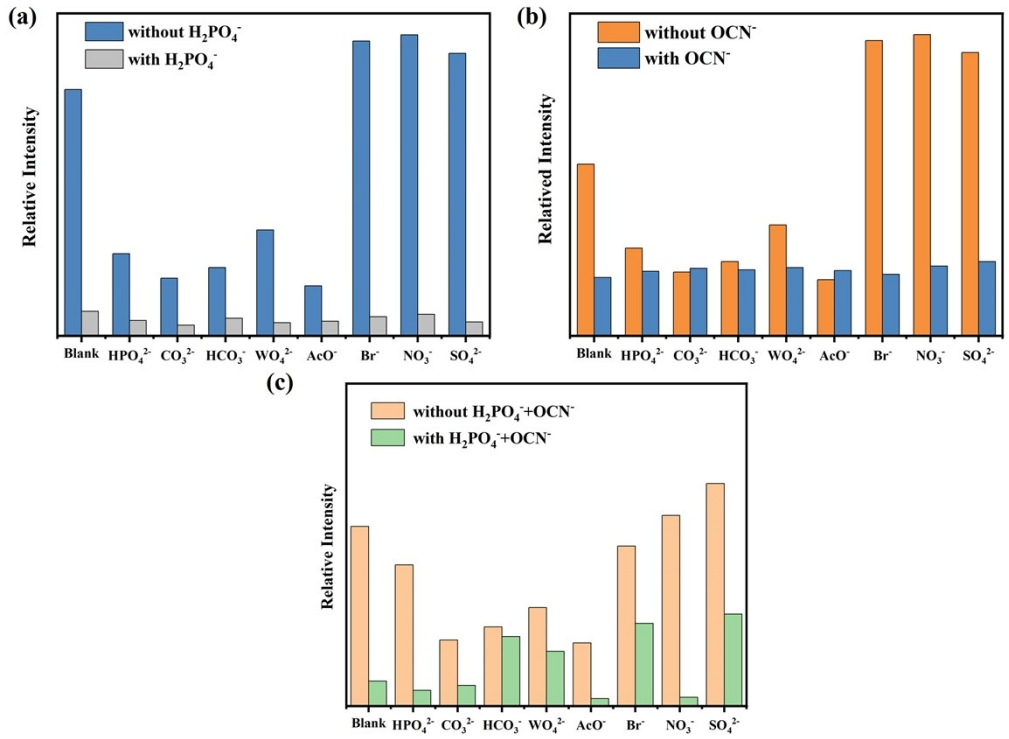

Fig. S11 Competitive experiments of **JXUST-47** in sensing (a) $H_2PO_4^-$, (b) OCN^-, and (c) $H_2PO_4^-$ and OCN^- with the other interfering substance.

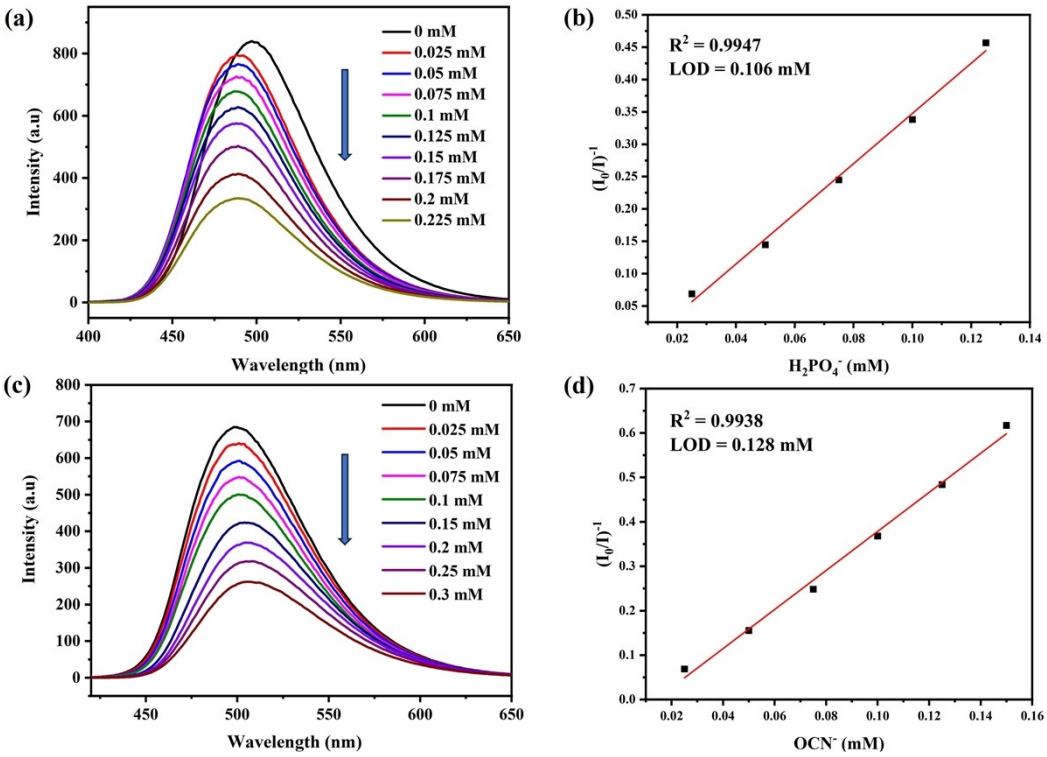

Fig. S12 Emission spectra of **JXUST-47** dispersed in DMF suspension with different concentrations for (a) $H_2PO_4^-$ and (c) OCN^- ions, and the linear relationship in a low concentration range between the fluorescence intensity of **JXUST-47** and the concentration of (b) $H_2PO_4^-$ and (d) OCN^- ions.

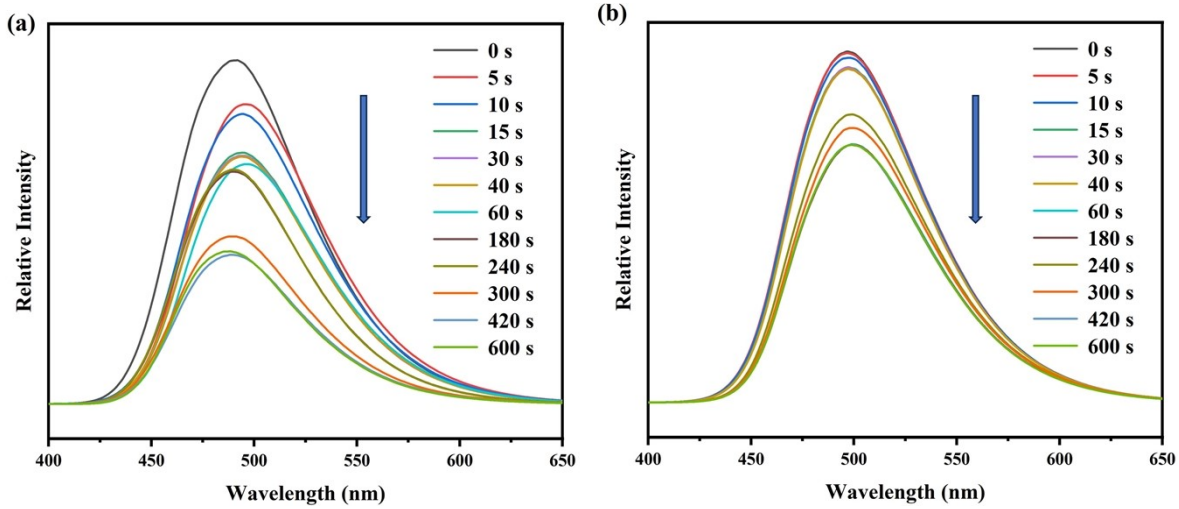

Fig. S13 Time-dependent emission spectra of the suspension after adding 0.2 M (a) $H_2PO_4^-$ and (b) OCN^-.

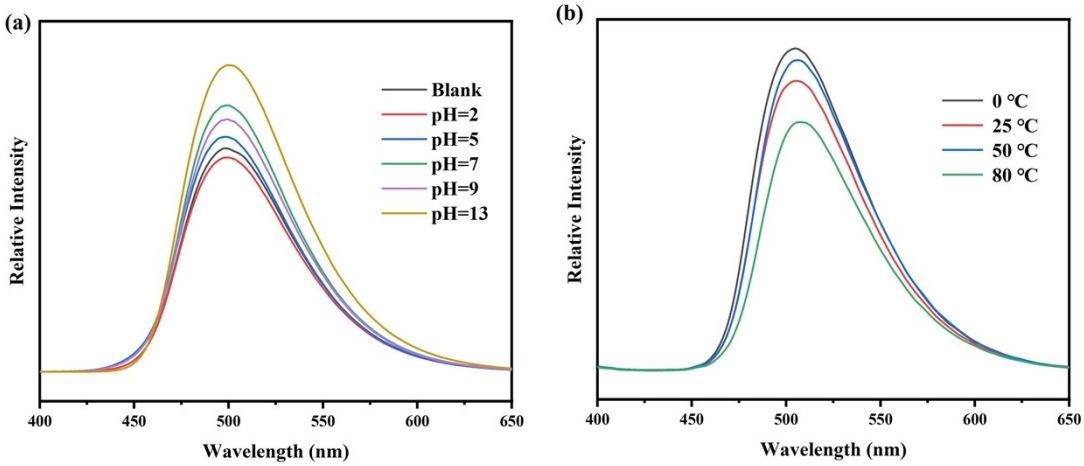

Fig. S14 The emission spectra of **JXUST-47** (a) in DMF aqueous solution with different pH values and (b) at different temperatures.

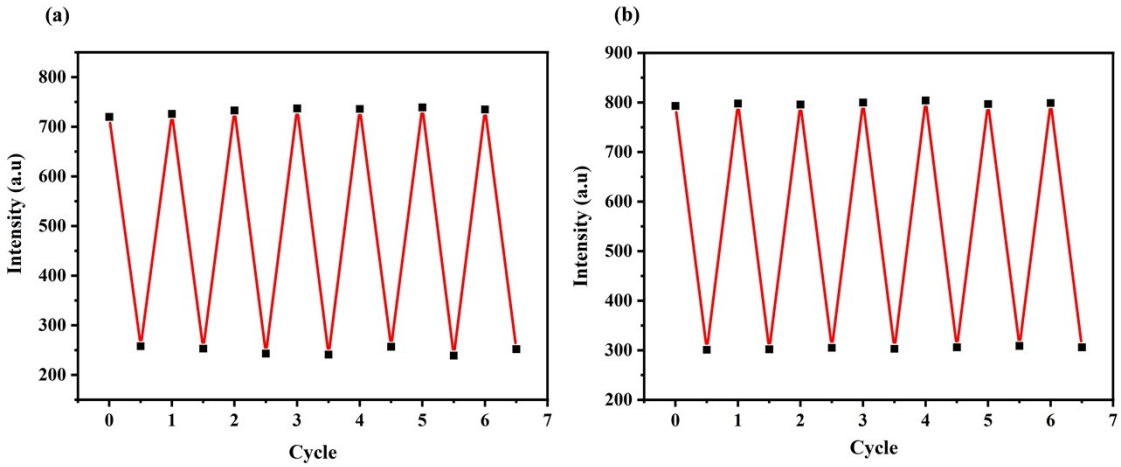

Fig. S15 Relative luminescent intensity of **JXUST-47** after seven cycles for (a) $H_2PO_4^-$ and (b) OCN^-.

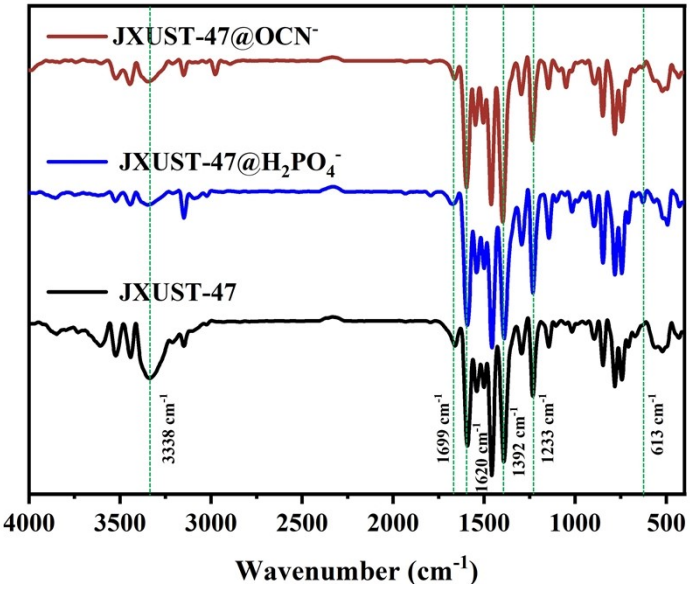

Fig. S16 The IR spectra of as-synthesized **JXUST-47** and **JXUST-47** after sensing $H_2PO_4^-$/OCN^-.

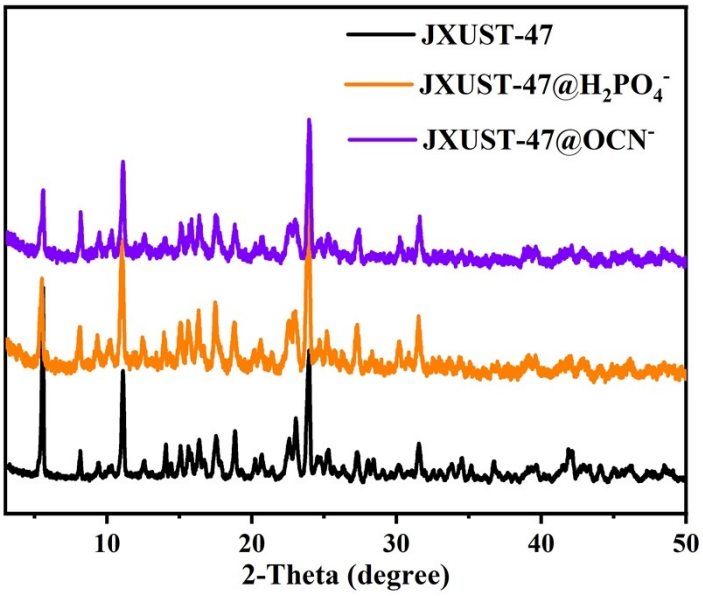

Fig. S17 The PXRD patterns of as-synthesized **JXUST-47** and **JXUST-47** after sensing $H_2PO_4^-$/OCN^-.

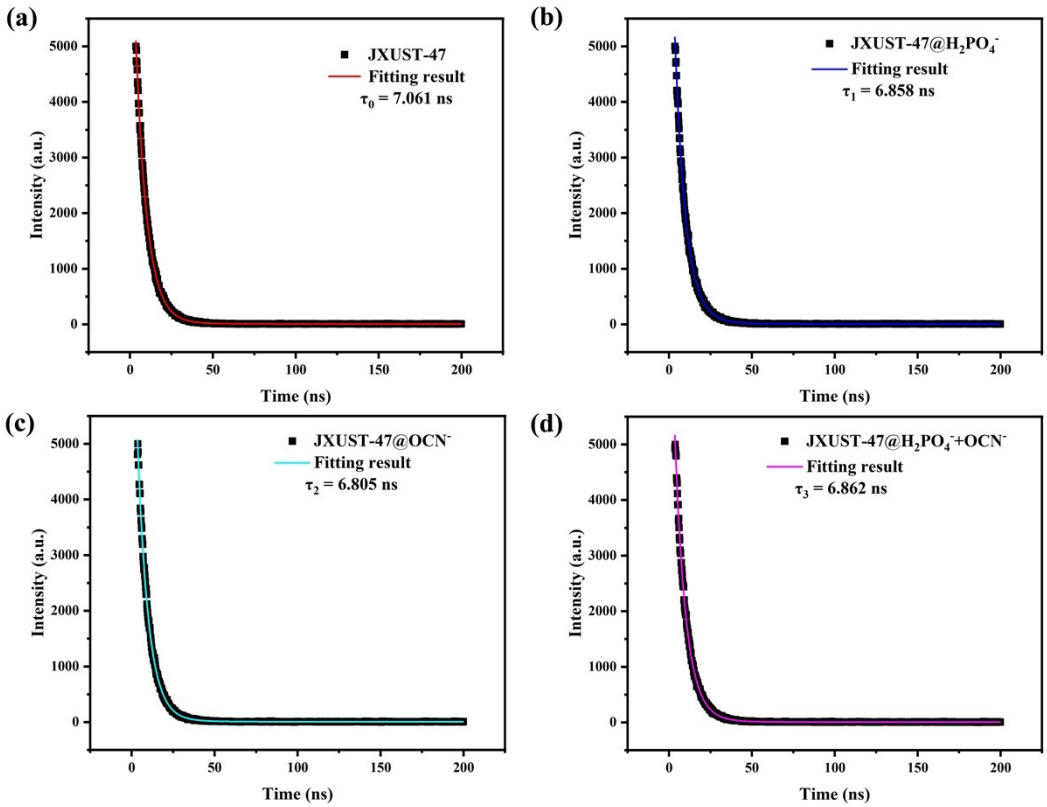

Fig. S18 The luminescence decay curves of (a) **JXUST-47**, (b) **JXUST-47**@ $H_2PO_4^-$, (c) **JXUST-47**@ OCN^- and (d) **JXUST-47**@ $H_2PO_4^-$+OCN^- at room temperature.

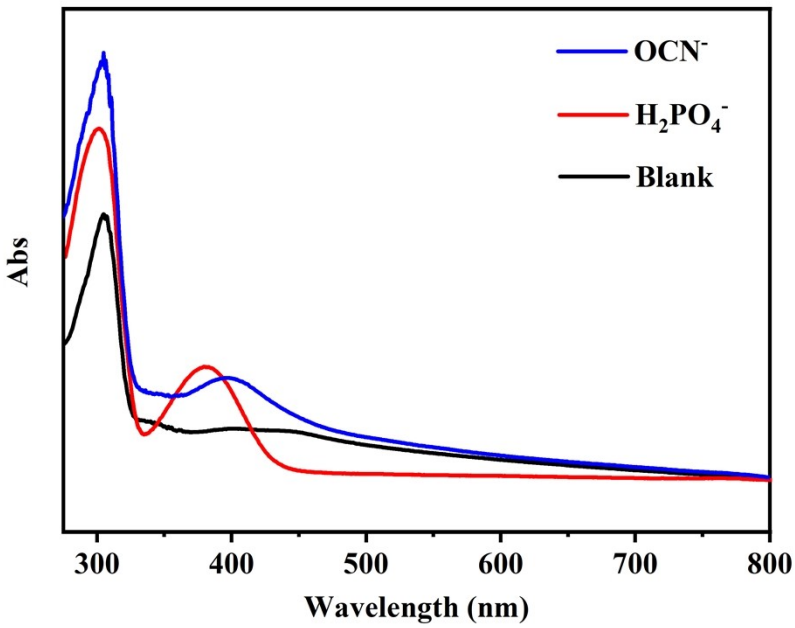

Fig. S19 The UV-vis absorption spectra of **JXUST-47** dispersed in DMF solution and **JXUST-47** dispersed in DMF solution after adding $H_2PO_4^-$ and OCN^-.

Table S1. Crystal data and structure refinements for **JXUST-47**.

Compound	**JXUST-47**
Formula	$C_{39}H_{23}N_7O_4SCd$
M_r	798.10
Temperature (K)	293(2)
Crystal system	triclinic
Space group	$P\bar{1}$
a (Å)	9.4237(11)
b (Å)	11.6946(13)
c (Å)	16.1030(17)
α (°)	82.624(5)
β (°)	83.013(5)
γ (°)	68.067(4)
V (Å^3)	1627.3(3)
Z	2
F(000)	804.0
D_{calc} (g cm^{-3})	1.629
μ (mm^{-1})	0.792
Reflections collected/unique	19017/5584
R_{int}	0.1686
R_1^a/wR_2^b [$I>2\sigma(I)$]	0.1032/0.1275
R_1^a/wR_2^b (all data)	0.1708/0.1453
GOF on F^2	1.074

$^aR_1 = \Sigma(||F_0| - |F_C||)/\Sigma|F_0|$; $^bwR_2 = [\Sigma w(|F_0|^2 - |F_C|^2)^2/(\Sigma w|F_0|^2)^2]^{1/2}$.

Table S2. Selected bond lengths (Å) and angles (°) for **JXUST-47**[a].

Cd1—O1	2.211(6)	Cd1—N3	2.325(7)
Cd1—O2	2.643(6)	Cd1—O4^{ii}	2.388(6)
Cd1—O3^{i}	2.268(5)	Cd1—N7^{iii}	2.483(7)
O3^{i}—Cd1—O2	139.3(2)	O3^{i}—Cd1—N7^{iii}	78.8(2)
O3^{i}—Cd1—N3	81.6(2)	N3—Cd1—O2	138.3(2)
O3^{i}—Cd1—O4^{ii}	102.9(2)	N3—Cd1—O4^{ii}	82.1(2)
O1—Cd1—O2	53.6(2)	N3—Cd1—N7^{iii}	117.7(3)
O1—Cd1—O3^{i}	159.3(2)	O4^{ii}—Cd1—O2	80.4(2)
O1—Cd1—N3	90.8(2)	O4^{ii}—Cd1—N7^{iii}	160.0(2)
O1—Cd1—O4^{ii}	95.1(2)	N7^{iii}—Cd1—O2	85.6(2)
O1—Cd1—N7^{iii}	88.0(2)		

[a]Symmetry codes: (i) x-1, y, z-1; (ii) -x+2, -y+1, -z+1; (iii) -x, -y+1, -z; (iv) x+1, y, z+1.

Table S3. Comparison of others work with **JXUST-47** for the fluorescence detection of $H_2PO_4^-$.

MOFs	Sensing medium	LOD	Interferences	Bio-imaging	Reference
UiO-66-NH_2	H_2O	0.73 μM	I^-, Br^-, Cl^-, ClO_4^-, AcO^-, SO_4^{2-}, HSO_4^-	–	S2
F-MOF	CH_3OH–H_2O	3.903 μM	$P_2O_7^{4-}$, SCN^-, AsO_4^{3-}, IO_3^-, AsO^{3-}, SO_4^{2-}, F^-, Br^-, NO_3^-, CH_3COO^-, PO_4^{3-}, HF_2^-, AsO_2^-, CN^-, HPO_4^{2-}	WI-38 cell	S3
Zn-DMBI	CH_3OH	1.3 μM	F^-, SO_4^{2-}, ClO_4^-, NO_3^-, I^-, TfO^-, BF_4^-, AcO^-, Br^-, OH^-, HCO_3^-, HSO_4^-	–	S4
JXUST-44	DMF	0.121 μM	F^-, Br^-, Cl^-, I^-, NO_3^-, SO_4^{2-}, WO_4^{2-}, HPO_4^{2-}, PO_4^{3-}	–	S5
JXUST-47	DMF	0.106 mM	HPO_4^{2-}, HCO_3^-, CO_3^{2-}, WO_4^{2-}, Br^-, SO_4^{2-}, AcO^-, NO_3^-	–	**This work**

References

S1. G. M. Sheldrick, Acta Crystallogr., *Sect. C: Struct. Chem.*, 2015, **71**, 3–8.

S2 R. Dalapati and S. Biswas, *Sen. Actuators B: Chem.*, 2017, **251**, 250–255.

S3. K. Naskar, A. K. Bhanja, S. Paul, K. Pal and C. Sinha, *Cryst. Growth Des.*, 2020, **20**, 6453–6460.

S4. S. Jindal and J. N. Moorthy, *Inorg. Chem.*, 2022, **61**, 3942–3950.

S5. Y. P. Li, J. H. Zhang, X. X. Zhang and S. J. Liu, *CrystEngComm*, 2023, **25**, 6424–6423.